International Journal of Homoeopathic Sciences

E-ISSN: 2616-4493
P-ISSN: 2616-4485
www.homoeopathicjournal.com
IJHS 2024; 8(2): 485-497
Received: 25-03-2024
Accepted: 26-04-2024

Neeladrisingha Das
Department of Molecular Endocrinology Laboratory, Biosciences and Bioengineering, Indian Institute of Technology Roorkee, Roorkee, Uttarakhand, India

Papu Kumar Naik
A) Department of Chemical Engineering, Indian Institute of Technology Guwahati, Guwahati, Assam, India
B) Department of Earth and Environmental Science, Parul Institute of Applied Sciences, Parul University, Vadodara, Gujarat, India

Chandrachur Ghosh
Department of Molecular Endocrinology Laboratory, Biosciences and Bioengineering, Indian Institute of Technology Roorkee, Roorkee, Uttarakhand, India

Anjali Raj
Molecular Endocrinology Laboratory, Department of Biosciences and Bioengineering, Indian Institute of Technology Roorkee, Roorkee, Uttarakhand, India

Debabrata Sircar
Plant molecular biology Laboratory, Department of Biotechnology, Indian Institute of Technology Roorkee, Roorkee, Uttarakhand, India

Tamal Banerjee
Department of Chemical Engineering, Indian Institute of Technology Guwahati, Guwahati, Assam, India

Partha Roy
A) Department of Molecular Endocrinology Laboratory, Biosciences and Bioengineering, Indian Institute of Technology Roorkee, Roorkee, Uttarakhand, India
B) Center for Indian Traditional Knowledge, Indian Institute of Technology Roorkee, Roorkee - 247667, Uttarakhand, India

Corresponding Author:
Partha Roy
A) Department of Molecular Endocrinology Laboratory, Biosciences and Bioengineering, Indian Institute of Technology Roorkee, Roorkee, Uttarakhand, India
B) Center for Indian Traditional Knowledge, Indian Institute of Technology Roorkee, Roorkee - 247667, Uttarakhand, India

Physico-chemical characterization, energy dynamics and anti-cancer efficacy of *Conium maculatum* homeopathic formulations against prostate cancer cell lines

Neeladrisingha Das, Papu Kumar Naik, Chandrachur Ghosh, Anjali Raj, Debabrata Sircar, Tamal Banerjee and Partha Roy

DOI: https://doi.org/10.33545/26164485.2024.v8.i2g.1176

Abstract
Background: Prostate cancer is a major global health concern with existing treatments often having severe side effects. Homeopathic treatments are considered safer alternatives, yet their efficacy and mechanisms are debated due to their highly diluted nature and the energy dynamics due to potentization.
Objectives: This study aims to characterize the physico-chemical properties and energy dynamics of *Conium maculatum* (CM) homeopathic formulations and evaluate their anti-cancer efficacy against DU145 prostate cancer cell lines.
Methods: Advanced analytical techniques like Transmission Electron Microscopy (TEM) and Atomic Force Microscopy (AFM) were used to characterize the nanoparticles in CM formulations. Energy distribution was assessed through molecular simulations. The anti-proliferative effects were evaluated using MTT assays to monitor cell viability across different dilutions.
Results: TEM and AFM analyses confirmed the presence of nanoparticles, with a decrease in size at higher dilutions. Molecular simulations showed increased energy states in diluted formulations, correlating with higher therapeutic efficacy. CM formulations demonstrated significant cytotoxic effects against DU145 cells, particularly at lower dilutions (MT, 6C, 12C).
Conclusions: The study provides empirical support for the physico-chemical properties and therapeutic potential of CM formulations in prostate cancer treatment, suggesting that homeopathic dilutions retain bioactive properties that can effectively inhibit cancer cell proliferation.

Keywords: Homeopathy, *Conium maculatum*, nano-particle, energy, prostate cancer

1. Introduction
Prostate cancer remains a major global health challenge, ranking as the second most common type of cancer among men and a leading cause of cancer-related mortality worldwide. The conventional treatment modalities for prostate cancer, such as surgery, radiotherapy, chemotherapy, and hormonal therapy, although effective, are often associated with significant adverse effects and substantial financial costs. As the global incidence of prostate cancer is expected to rise significantly, there is an urgent need for alternative therapeutic strategies that are both effective and have fewer side effects [1].
In this context, complementary and alternative medicine (CAM) options, particularly homeopathy, are gaining popularity. Homeopathy is practiced widely across the globe, with a notable presence in South Asia, Western Europe, and increasing acceptance in North America. Despite its widespread use, homeopathy has been surrounded by controversies, particularly concerning its principles of extreme dilutions and potentization. Critics argue these dilutions surpass Avogadro's number, potentially leaving no molecules of the original substance, which challenges conventional scientific paradigms [2-3].
Recent scientific efforts aim to bridge the gap between traditional homeopathic practices and modern scientific standards. Studies have begun to explore the physico-chemical properties of homeopathic solutions, suggesting that these might possess unique nanoparticulate characteristics that could underlie their therapeutic potency. These nanoparticles are believed to be formed through the process of succussion; a systematic shaking used in homeopathy to increase a preparation's potency [4].

However, the precise mechanisms through which potentization and energy distribution contribute to the therapeutic efficacy of homeopathic remedies remain poorly understood. While some studies have started to elucidate these phenomena [5-6], the scientific explanations for how such processes might function at the molecular level remains unclear.

This study focuses on *Conium maculatum* (CM), a homeopathic preparation traditionally used for treating glandular and cancerous conditions, including prostate and breast cancer. Despite anecdotal benefits reported in homeopathic literature, rigorous scientific evaluations to substantiate these claims, particularly in oncological applications, are scant. Our research employs advanced physico-chemical analysis techniques such as transmission electron microscopy (TEM) and atomic force microscopy (AFM) to investigate the nanoparticulate nature of CM and assess its potential energy distribution due to the potentization process. Innovatively, we apply a novel energy simulation method to predict energy differences by applying external force under different dilutions. This approach may provide crucial insights into the energy distribution during potentization, offering some much-needed scientific clarity on the operational mechanisms of homeopathic dilutions. Additionally, we explored the anti-proliferative effects of CM on the prostate cancer cell line to establish a preliminary scientific basis for its application in cancer treatment.

By demonstrating the physical properties and cellular impacts of CM, this study seeks to provide a critical scientific foundation that could lead to broader acceptance and integration of homeopathy within the realm of cancer therapeutics.

2. Materials and Methods

2.1 Chemicals and Reagents

Human prostate cancer cell lines (DU145 and LnCAP cells) and human embryonic kidney cells (HEK293 cells) were procured from the National Centre for Cell Science (NCCS), Pune, India. All cell culture reagents were sourced from GIBCO (Invitrogen, USA). MTT (3-(4,5-dimethyl-2-thiazolyl)2,5-diphenyl-2H-tetrazolium bromide), streptomycin, penicillin, cell culture grade DMSO, 5-Fluorouracil (5-FU), and other analytical grade chemicals were obtained from HiMedia (Mumbai, India). CM homeopathic formulations were provided by Hahnemann Publishing Co. Pvt. Ltd. (HAPCO, Kolkata, India), batch number HM180077.

2.2 Cell Culture

All cells, i.e., DU145, LNCaP, and HEK293, were cultured and grown in RPMI1640 medium (Himedia, Mumbai, India) supplemented with 10% (v/v) fetal bovine serum (GIBCO, Invitrogen, USA) and 1% antibiotics (100 mg/ml streptomycin and U/ml of penicillin) (Himedia, Mumbai, India). Cells were maintained in a humidified incubator at 5% CO2 and 37 °C. All experiments were performed with cells from their lowest passage numbers.

2.3 MTT Assay

The MTT assay was performed according to the protocol described previously [7]. Briefly, 5 X 10^3 to 7 x 10^3 cells were seeded in a 96-well plate. After 24 hours of incubation, the culture media was replaced with fresh media containing different dilutions of CM (MT, 6C, 12C, 30C, and 200C) as test material. The cells were then incubated for 24 hours in a humidified incubator at 5% CO_2 and 37 °C. At the end of the incubation, 20 µl of MTT reagent (5 mg/ml) was added and allowed to incubate for another 4 hours. Then, 150 µl of DMSO was added to solubilize the formazan crystals in each well. Absorbance was measured at 570 nm using a multimode plate reader (Fluostar Omega, BMG LabTech, Germany).

2.4 Computational Methods for Energy Calculations

Computational methods were employed using Gaussian 05 and Gaussian 09 [8] to draw and optimize the geometries of the top five molecules identified through LC/MS studies: conhydrin (COH), coniceine (COC), coniine (COI), pseudoconhydrine (PSE), and n-methylconniine (NME). The optimized geometry was obtained at the B3LYP/6-31+g(d) level of theory [9]. Partial charges were obtained using the restrained electrostatic potential (RESP) charge derivation method [10] of AMBER 14 [11]. The generalized amber force field (GAFF) parameters functional form [12] using ANTECHAMBER module [13] of AMBER 14 was used to generate the force field parameters of the simulation systems. The detailed simulation method is described in Supplementary Method1 (Supplementary File).

2.5 Physico-chemical Characterization

The average size of the particles was determined by transmission electron microscopy (TEM) using a FEI Tecnai G2 20 S-Twin (FEI, Hillsboro, OR, USA) operating at 60 kV. Formulations were placed on formvar-coated 200 mesh TEM grids (grid size: 97 mm) (Ted Pella, Inc., Redding, CA, USA). Excess suspension on the grid was removed using fine needles and brushes. Before imaging, samples were air-dried for 8 hours. Surface morphology of the CM formulations was analyzed using a scanning probe microscope (SPM) (NT-MDT-NTEGRA, Moscow, Russia) with a position sensitivity of 2 µM and a resonance frequency of 115-190 kHz.

3. Results

3.1 Active constituents of CM homeopathic MT

To identify the active constituents of the CM homeopathic formulations, liquid chromatography–mass spectrometry (LC-MS) of the MT was carried out. Our result showed that the MT of CM contained several bio-active phytochemicals including- 2methylpiperidine, coniine, coniceine, N-methylconniine, conhydrin, conhydrinone, pseudoconhydrine, conmaculatin, N, N- Dimethylconine and γ-coniceine. Figs. 1(A) and (B) show the chromatogram and the structure of the active phytoconstituents present in CM, respectively.

3.2 Diluted formulation along with externally applied force exerts more energy than undiluted formulation without force

In order to establish the energy theory of homeopathy i.e. imparting energy by applying external force while preparing the dilutions, we measured the net energy as well as the inter-molecular energy of the major constituents of CM formulation by molecular simulations. We simulated two conditions, System1 (S1) and System2 (S2), to apply external force. S1 contains 100 molecules, representing a concentrated version, while S2 comprises 10 molecules,

reflecting a diluted version (Fig.1C). The detailed calculations of S1 and S2 are described in Supplementary Method1 (Supplementary File)**.** Various energy calculations are described hereunder:

3.2.1 Nonbonded interaction energy (IE)
The nonbonded interaction energies (IE) between different molecules in each simulation system include electrostatic and van der Waals (vdW) interactions (Table 1). System S2 displayed more favorable interactions than System S1, with the highest total interactions occurring between conhydrin and pseudoconhydrine, followed by N-methylconniine (Fig. 2A). The vdW interactions predominated over electrostatic interactions due to molecular size, leading to steric hindrance that reduced electrostatic effects. Notably, all molecule pairs had total interaction energies ranging from -15 to -30 kJ/mol, except for the COH-PSE pair, ensuring uniformity and stability across the simulation. Upon applying external force to System S2, it accumulated more energy, enhancing IE across all pairs. Table 2 details the initial and final energy levels of the system, including the net energy increase, with potential energy predominating over kinetic energy.

3.2.2 Hydrogen bonding analysis
Fig. 2B represents the average number of hydrogen bonds per protein molecule of the system for the last 10 ns trajectory at the end of the production run of the simulation. A cut off distance of 3.5 Å with a cut off angle of 180° was used for hydrogen bond calculation. For each system, the shown fraction of H-bond was normalized and averaged in the system per molecule in order to compare distances and energies relative to each other. As shown in Fig. 2B for both the systems the highest fraction of hydrogen bond interactions occurs between COH-PSE pairs. This also supports the interaction energy. The main cause for a larger contribution of COH-PSE pair hydrogen bonds is the presence of an additional OH functional group in both cases. The average H-bond numbers of COC-COI and COC-NME are insignificant. System S1 has a higher value of H-bonding than system S2 because the external force may hinder the ability of H bond formation, despite S2 having higher interaction energy.

3.2.3 Radial distribution function (RDF)
Radial distribution functions (RDF) evaluate the structural arrangements of molecules within simulation systems, as shown in Figs. 3 and 4 for S1 and S2, respectively. Nitrogen and oxygen atoms were selected and labeled as per Fig. 1A. The first tallest RDF peaks, near 2.5 Å, correspond to intermolecular hydrogen bond distances, with a second peak indicating non-hydrogen bonded intramolecular distances [Figs. 3, 4(A-E)]. Notably, COH and PSE interactions across multiple regions produce wavy peaks (Figs. 3A, 3D), with prominent COH-PSE interactions highlighted by both H-bonded analysis and intermolecular energies. Conversely, Fig. 3B reveals a weak first peak, suggesting minimal solvation interaction, whereas Figs. 3C and 3E demonstrate strong single-zone interactions. Similar patterns are observed in System S2 (Figs. 4A, 4D), indicating robust interactions for COH and PSE across multiple regions. Comparative analysis between Figs. 3B and 4B shows insignificant interactions for COC moieties, weakening further with external force. Additionally, the radial distribution function magnitude or g(r) increases with force in System S2, suggesting enhanced dispersion and intermolecular energy influence, while intramolecular interactions within the same species are minimal.

3.2.4 Spatial Distribution Function (SDF)
Spatial Distribution Function (SDF) plots illustrate the average density distribution of protein molecules around central reference molecules, as shown in Figs. 5 and 6 for systems S1 and S2, respectively. In S1, COH centrally attracts electron clouds for closer, more uniform interactions (Fig. 5A), whereas proteins around COC are loosely distributed, showing weak g(r) peaks in RDF plots (Fig. 5B). In contrast, COH, PSE, and NME exhibit closer distributions compared to COC and COI. In S2, electron densities are looser and more spread out due to external energy and dilution, dispersing the electron cloud more effectively (Fig. 6). Figs. 5A and 5D reveal COH and PSE centrally located, with other molecules more compactly arranged than COC, COI, and NME (Figs. 5B, 5C, 5E). These observations indicate that the absence of force leads to short-range interactions, whereas the application of force results in long-range interactions, supporting the hypothesis that force-enhanced diluted systems interact more energetically and efficiently, improving the carrier capacity for molecules.

3.2.5 Self-diffusion coefficient (D)
Estimating the self-diffusion coefficient provides an accurate measure of the overall mobility of different species in phase equilibrium. The Einstein equation is used to determine the self-diffusion coefficients of various species (Eq. 1) [14-17].

$$D = \frac{1}{6}\lim_{t\to\infty}\frac{d}{dt}\left[\left|r_i(t) - r_i(0)\right|^2\right] \quad \text{(Eq. 1)}$$

Where $r_i(t)$ and $r_i(0)$ are the positions of the target atom of the molecule at time t and 0, respectively. These values were derived from the mean square displacement of the molecule in the system. We computed the diffusivity value at three intervals during the entire simulation run, at 0−10 ns, 40-50 ns, and 90−100 ns, respectively. For system S1, at the beginning of the simulation, the diffusivity of all the species shows a similar trend. The value decreases only at the end of the simulation run (90−100 ns). Table 3 shows the diffusion coefficient of each species of both systems and it reveals that for system S2, these values are relatively low in the presence of external force. This shows that the individual molecules diffusivity is somewhat higher in system S2. Smaller diffusivity value molecules result in higher relative stability within the system, implying their movement in the system is uniform. Table 3 exhibits that COH and PSE molecules have lower coefficient values at the end of the simulation. This shows higher interaction between them than other molecules.

3.3 Physico-chemical characterization of *Conium maculatum* homeopathic formulation
After assessing the energy profiles of both diluted and undiluted conditions, we examined the physicochemical properties of the CM mother tincture (MT) and its various dilutions to verify their nanoparticulate characteristics.

Transmission electron microscopy (TEM) and atomic force microscopy (AFM) images illustrate the structural changes at different dilutions (Fig. 7A and 7B). In the mother tincture, particles were nano-clustered, averaging about 0.5 µm (Fig. 7A). With increasing dilutions, the nanoclusters were observed to decrease in size and become more individualized. Specifically, in the 6C dilution, clusters were reduced to an average size of ~0.1 µm, and further diminution was noted in the 12C and 30C dilutions, with sizes approximately 30 nm and 10 nm, respectively. However, the underlying causes for these size reductions in the 12C and 30C dilutions remain unclear, as particles were already individualized in the 6C dilution.

Homeopathic remedies are typically administered via glucose balls, which necessitated further investigation into any changes in particle size once incorporated into these carriers. AFM analysis of the glucose balls doped with the homeopathic formulations showed that the particle size of the CM mother tincture on the glucose balls was around 1.6 µm. Consistent with the TEM findings, a gradual size reduction was observed in the glucose balls as the dilutions increased (Fig. 7B), with average particle sizes recorded at 300 nm for 6C, 100 nm for 12C, and 30 nm for 30C. This evidence confirms the nano-particulate nature and progressive individualization of the particles in diluted CM formulations—6C, 12C, and 30C.

3.4 *Conium maculatum* (CM) formulation exerts an anti-proliferative effect on prostate cancer cells.

Homeopathic formulations, including CM (*Conium maculatum*), typically use ethanol as the active solvent. To assess cytotoxicity, we first evaluated various ethanol dilutions—1:2, 1:5, 1:10, 1:15, and 1:20—given that CM MT, 6C, 12C, 30C, and 200C contain 60%, 91%, 91%, 91%, and 91% v/v ethanol, respectively, as per manufacturer labels (Fig. 8A). Ethanol proved highly cytotoxic to DU145, LNCaP, and HEK293 cell lines at 1:2 and 1:5 dilutions ($p < 0.05$), but was safe at higher dilutions, establishing 1:10 as the base concentration for further testing. Subsequently, the cytotoxicity of CM potencies (MT, 6C, 12C, 30C, and 200C) was tested in RPMI media at dilutions of 1:10, 1:25, 1:50, and 1:100, and assessed on DU145 cell lines over 24 hours in a dose-dependent manner. Results showed that MT, 6C, and 12C significantly reduced cell viability at a 1:10 dilution, whereas 30C and 200C were less effective (Fig. 8B). The IC50 values for MT, 6C, and 12C were approximately 1:42±0.022, 1:32±0.024, and 1:23±0.030, respectively, as documented in Table 4. These findings confirm the anti-proliferative properties of selected CM formulations, leading to their selection for deeper investigation at their respective IC50 dosages.

To further validate these findings, we conducted morphological assessments using an inverted phase-contrast microscope (Vert.A1, ZEISS, Germany) after 24 hours of treatment with CM MT, 6C, and 12C. The treated cells displayed significant morphological changes; those treated with CM MT showed reduced adherence and altered morphology, while cells treated with 6C appeared shrunken, rounded, and loosely adherent (Fig. 8C). These observations suggest that CM formulations, particularly at lower potencies, effectively induce cytotoxic effects in DU145 cell lines without apparent side effects, supporting their potential for therapeutic applications in cancer treatment.

4. Discussions

Homeopathic medicine, widely adopted for its holistic approach, is employed across numerous communities globally, deriving from natural sources that often render it safer compared to conventional therapies. Despite the advances in modern medicine, the underlying mechanisms and principles of homeopathy, such as dilutions and potentization, remain subjects of debate within the scientific community. Although homeopathy is becoming increasingly popular in many developing countries, including those in Europe, there remains a substantial need for rigorous scientific investigations to substantiate its claims [18]. In this study, we have embarked on exploring the physicochemical properties and energy dynamics of homeopathic drugs, shedding light on the potential mechanisms and the enigmatic relationship between energy and homeopathic dilutions. Additionally, we also explored the therapeutic potential of *Conium maculatum* (CM) homeopathic dilutions.

Conium maculatum (CM), utilized in homeopathy to address various ailments such as glandular enlargements and tumors in organs like the prostate, testes, ovaries, and breasts, is also recommended for women experiencing climacteric symptoms [19]. Motivated by these uses, our study aimed to examine the potential anti-cancer effects of CM on prostate cancer, alongside its physicochemical and energetic characteristics. Historically, multiple hypotheses have been suggested regarding the operational principles of homeopathic drugs, such as the nano-particulate nature of the source drug and theories like water clusters or Quantum coherence domain [20-21]. Our research aligns with these perspectives, revealing the nano-particulate nature of CM formulations at specific dilutions, although the origin of these particles remains undefined. Unlike previous studies where nanoparticles were also detected in control samples, our findings through Transmission Electron Microscopy (TEM) indicated that such particles were absent in our potentized controls, suggesting a direct link between the potentization process and nanoparticle formation. In studies by Wani *et al.* [22] and Klein and Wolf [23], homeopathic formulations of *Terminalia chebula*, were found to contain nanoparticles even at a potency of 6C, with mother tinctures exhibiting a nano-clustered structure. Similarly, Baumgartner *et al.* [24] observed a consistent presence of nanoparticles in commercially utilized homeopathic drugs. Our results complement these findings, showing nano-particulate formations within CM formulations at 12C and 30C dilutions, while our potentized controls devoid of nanoparticles contrast the findings by Klein and Wolf, suggesting a nuanced interplay between preparation techniques and nanoparticle formation. Despite the observed individualization of particles at 6C dilutions and the clustering in the mother tincture, the therapeutic implications of these physical states remain speculative yet promising for enhancing cytotoxic effects.

The transmission of energy during the dilution or potentization of homeopathic drugs, while a widely held notion, lacks substantial empirical support. Homeopathic potentization typically involves sequential dilutions and vigorous shaking, purportedly infusing energy into the preparations and enhancing their therapeutic efficacy [25]. In our investigations, using condition-based simulation models, we established distinct energy patterns associated with CM formulations. The initial simulation phase identified the active components of CM, which were consistent with those reported in earlier studies, thus corroborating the

biochemical similarity between the mother tincture and CM extracts [26-27]. Furthermore, our analysis of nonbonded interactions, hydrogen bonds, radial and spatial distribution functions illustrated an increased energy profile in formulations subjected to potentization, supporting the hypothesis that homeopathic drugs operate via enhanced energetic states.

Despite these advancements, the therapeutic relevance of CM, particularly its anti-cancer potential, corroborated by numerous case studies and scientific reports, underscores its significance in treating various physiological disorders, including cancer [28-30]. In accordance with these findings, our experimental data from in vitro studies provided empirical evidence of CM's cytotoxic effects on prostate cancer cells, affirming its potential utility in prostate cancer treatment.

This study significantly advances our understanding of homeopathic remedies, particularly through the lens of nano-particulate and energy dynamics. However, the complexity of the interactions at play and the preliminary nature of our findings highlight the need for further comprehensive studies. Advanced simulation techniques and extensive experimental validations are crucial to elucidate the mechanisms through which these remedies exert their effects, potentially paving the way for their integration into mainstream medical practices.

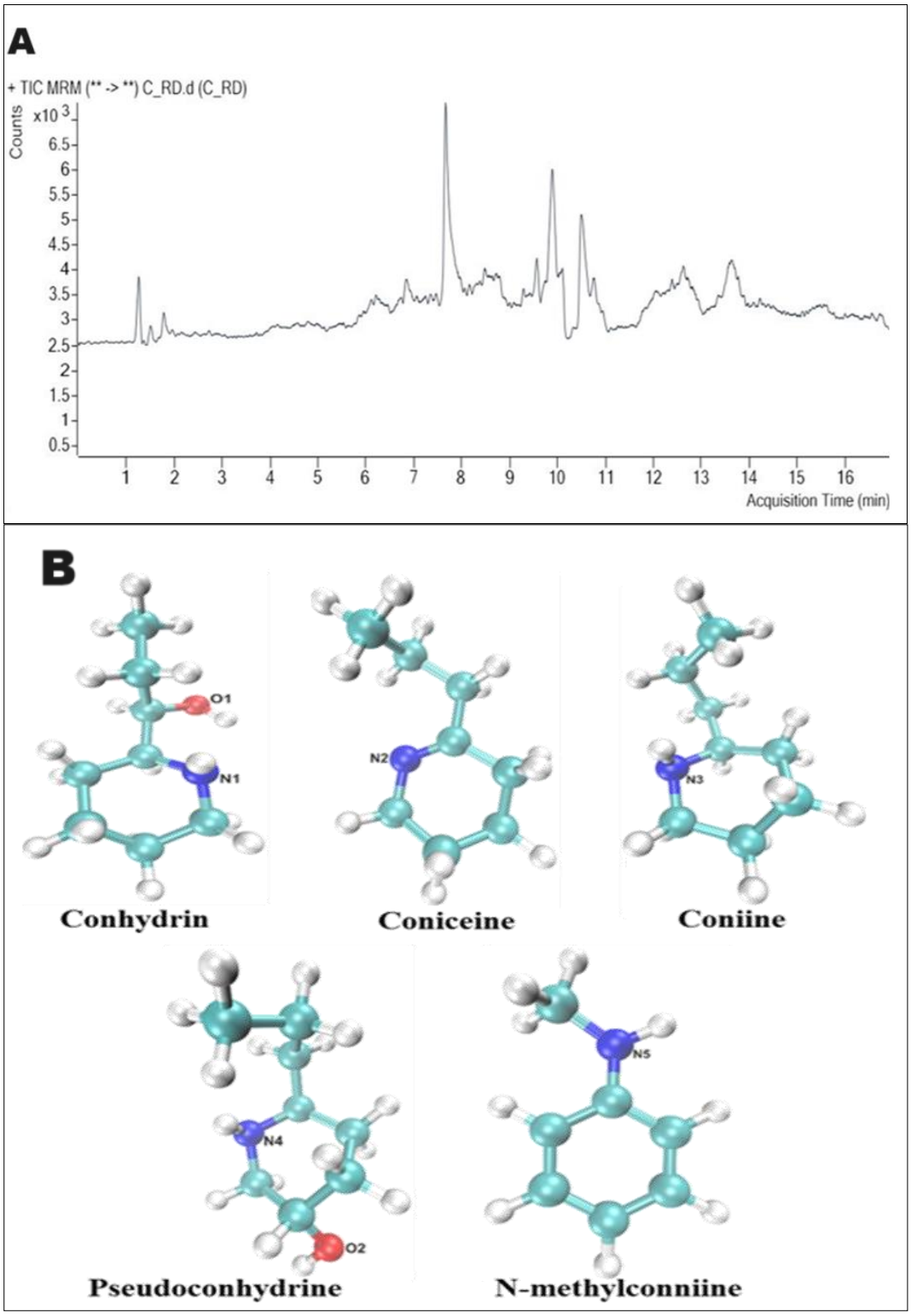

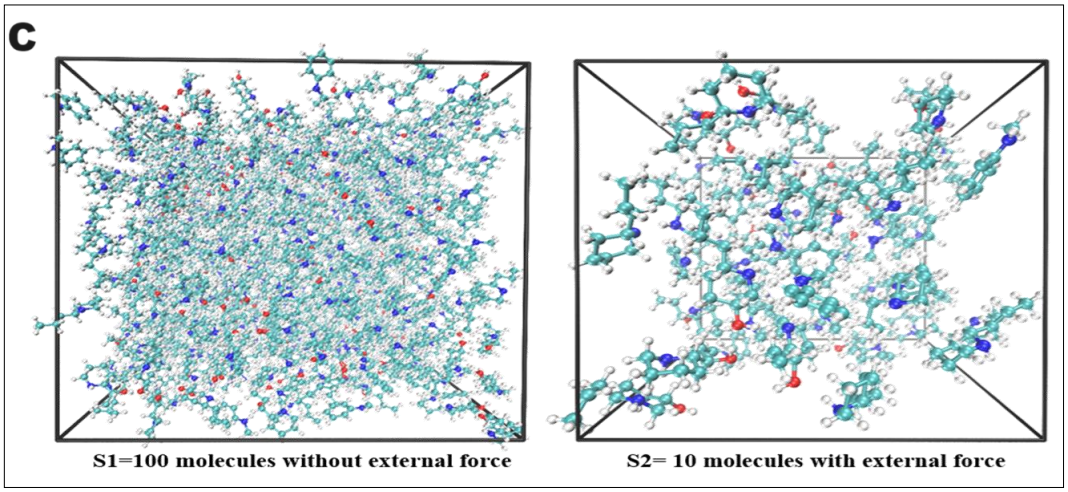

Fig 1: Identification of major constituents of CM and simulation conditions. (A) Chromatogram of LC/MS of the MT of CM shows various phytochemicals in the sample. (B) Optimized 3-dimensional structure of top five active phytochemicals present in the MT of CM. (C) Molecular simulation condition setting in which one case (left image) shows the condition having 100 molecules and without any applied force (S1). Whereas the second case (right image) shows the condition of having 10 molecules with applied external force (S2).

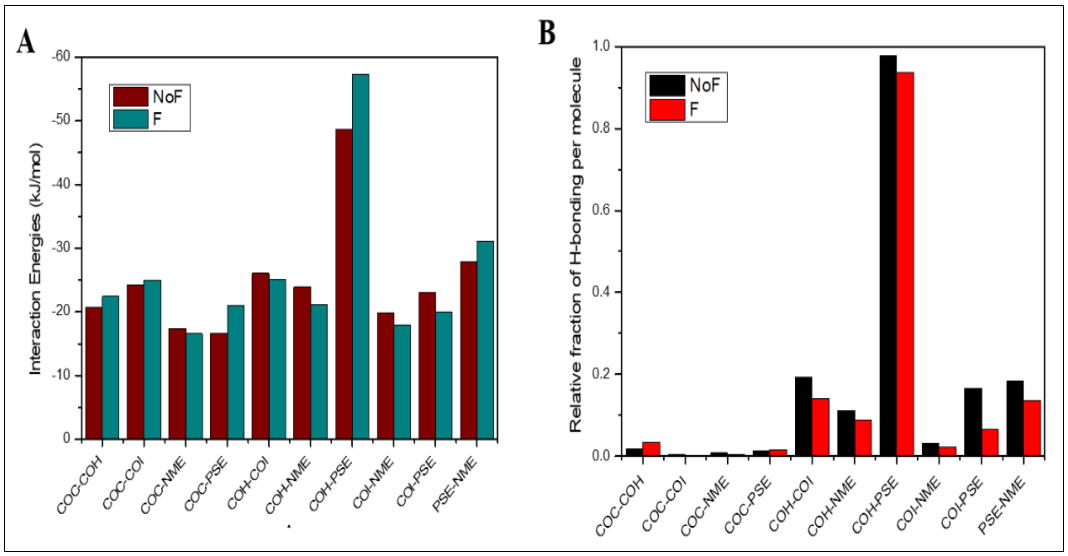

Fig 2: Energy distribution in the system. (A) Comparison of the total interaction energy between different species of both the systems (S1 and S2). (B)- Comparison of the average H-bonds between different species of both the systems (S1 and S2). Conhydrin, COH; coniceine, COC; coniine, COI; pseudoconhydrine, PSE; n-methylconniine, NME.

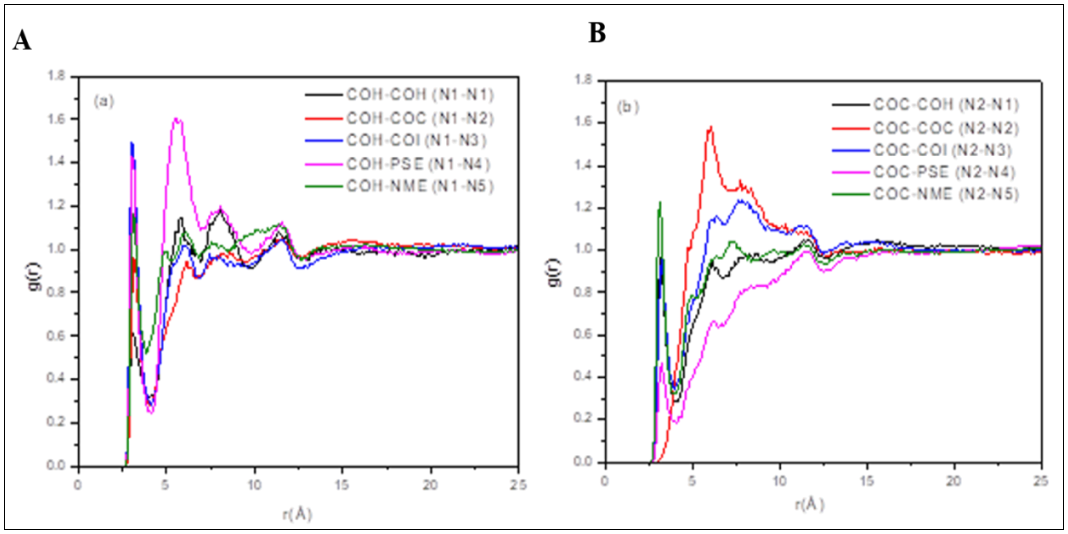

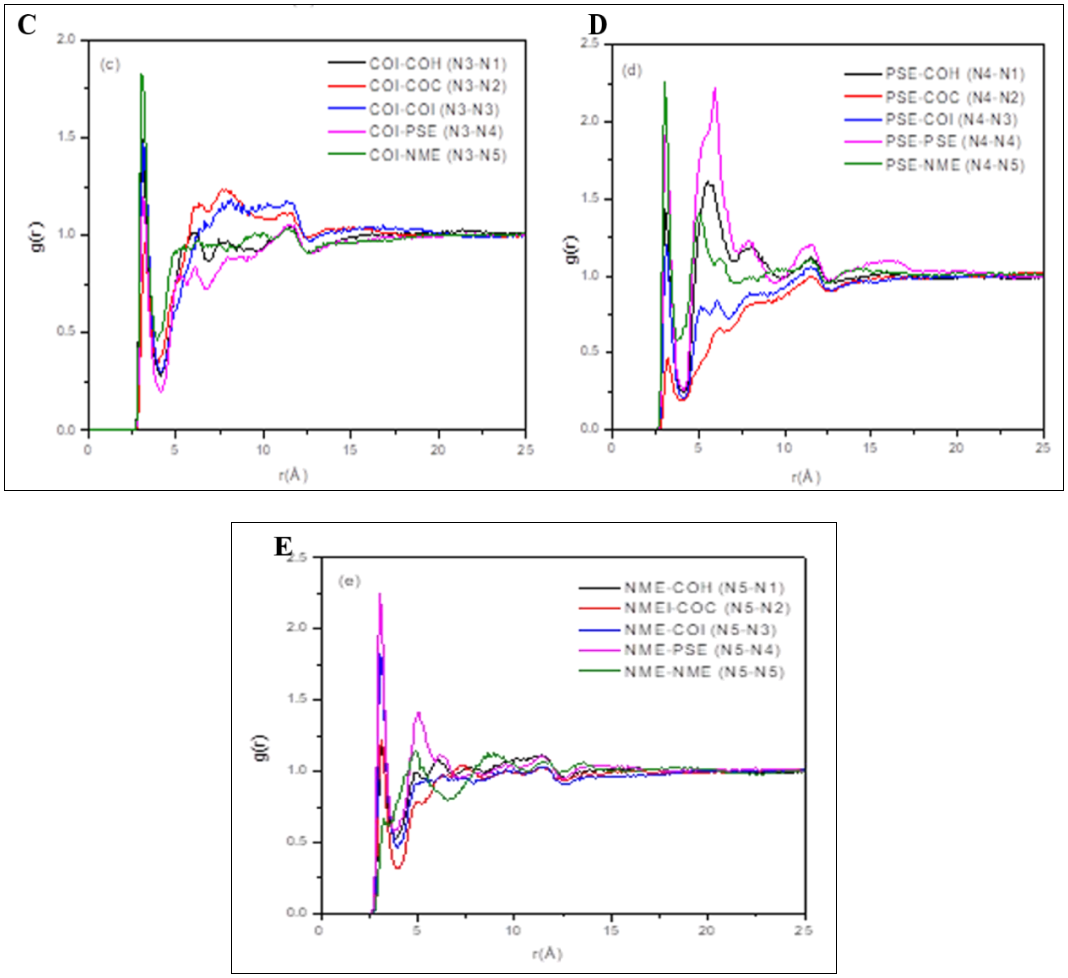

Fig 3: Atom−atom RDF plots between different molecules of system S1. (A) Conhydrine (COH), (B) Conicene (COC), (C) Coniine (COI), (D) Psedoconhydrine (PSE) and (E) N-methylconniine (NME) with other molecules obtained at 100 ns.

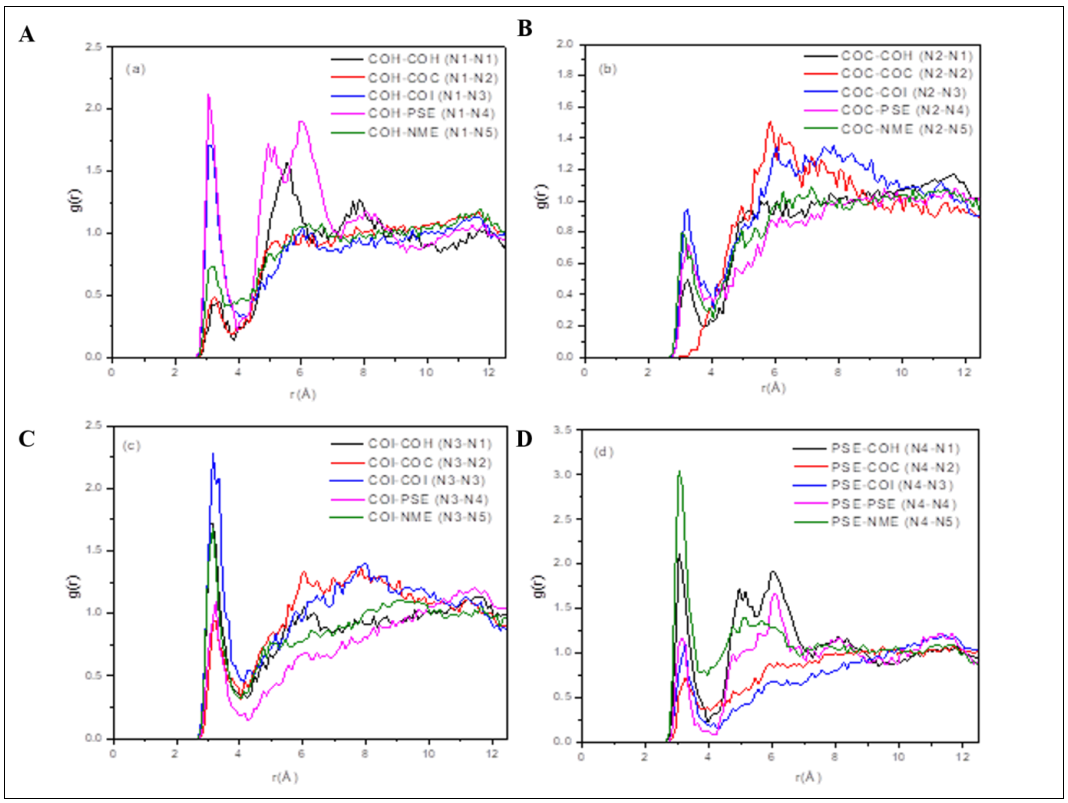

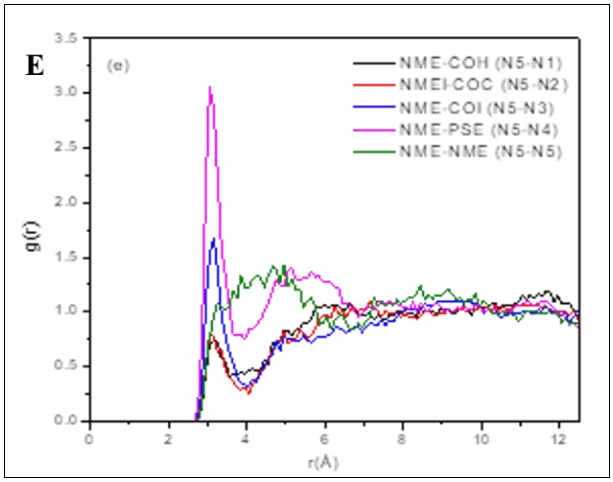

Fig 4: Atom−atom RDF plots between the different molecules of system S2. (A) Conhydrine (COH), (B) Conicene (COC), (C) Coniine (COI), (D) Psedoconhydrine (PSE) and (E) N-methylconniine (NME) with other molecules obtained at 100 ns.

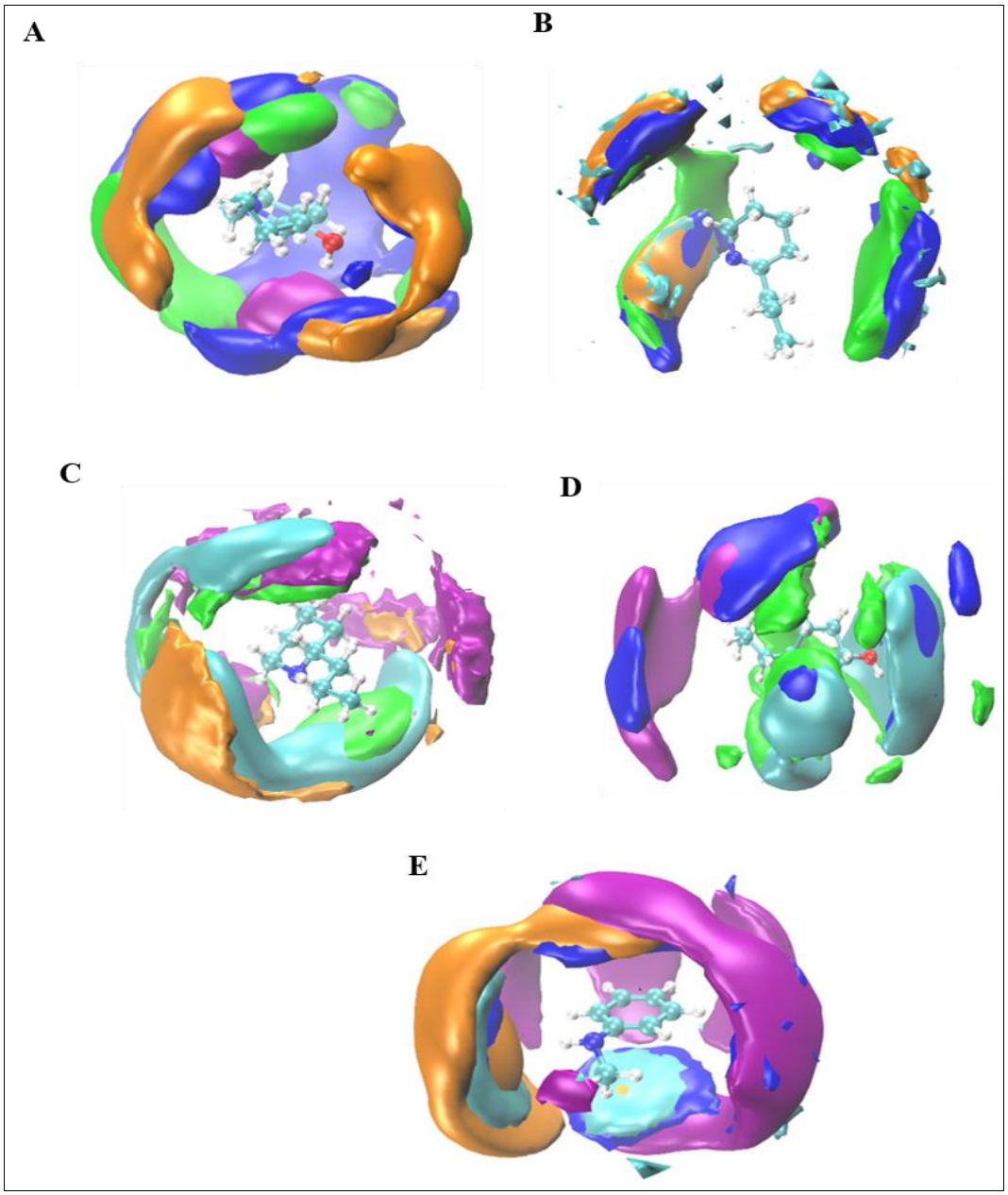

Fig 5: Spatial Distribution Function (SDFs) of different molecules around other individual molecules for system S1 (100 molecules without external force). In respective figures center position was occupied by (A) COH; (B) COC; (C) COI; (D) PSE and (E) NME. Cyan, purple, blue, orange, and green surfaces refer to Conhydrine (COH), Conicene (COC), Coniine (COI), Psedoconhydrine (PSE) and N-methylconniine (NME) respectively.

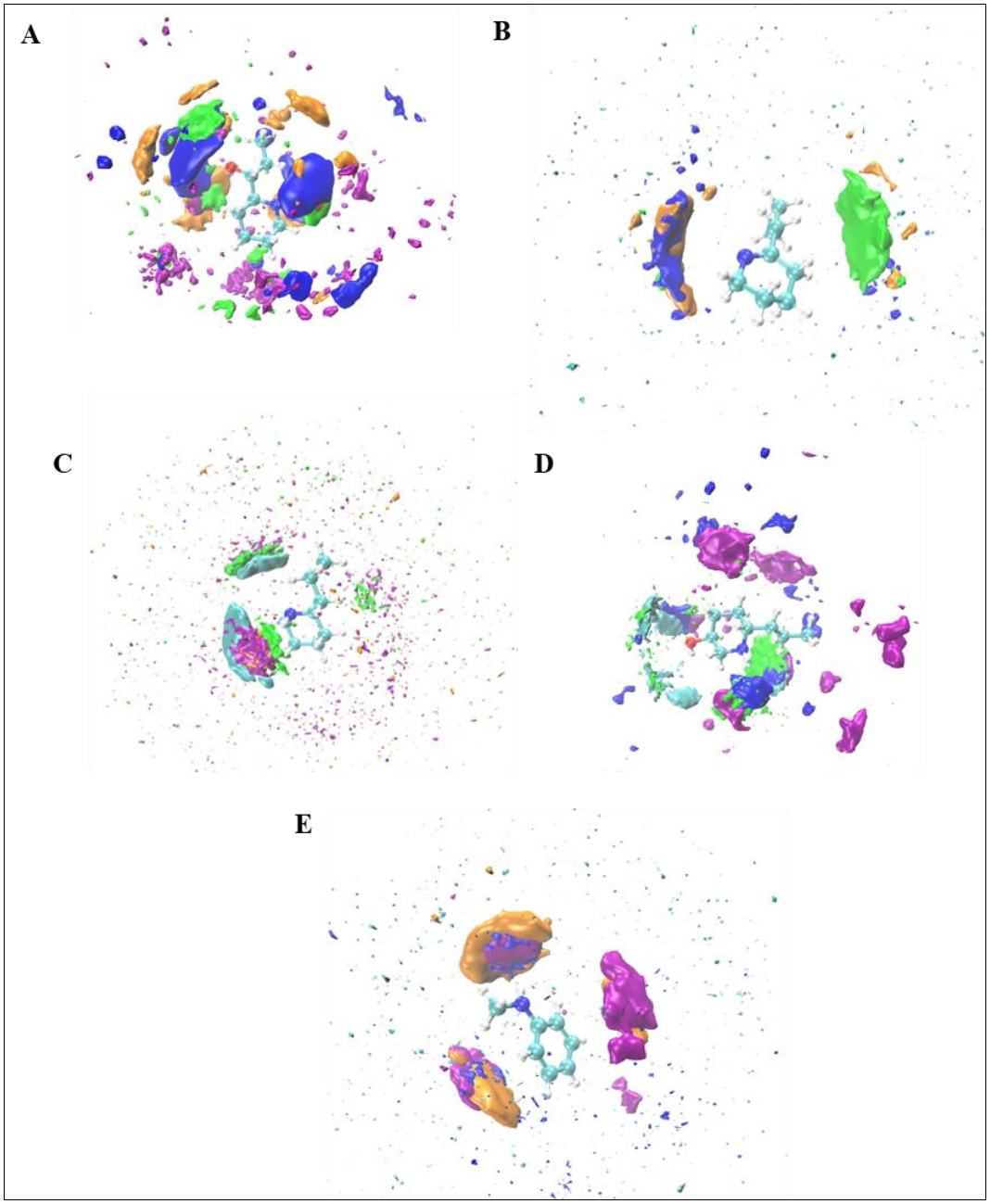

Fig 6: SDFs of different molecules around others for system S2 (10 molecules with external force). In respective figures center position was occupied by (A) COH;(B) COC; (C) COI; (D) PSE and (E) NME. Cyan, purple, blue, orange, and green surfaces refer to Conhydrine (COH), Conicene (COC), Coniine (COI), Psedoconhydrine (PSE), and N-methylconniine (NME), respectively.

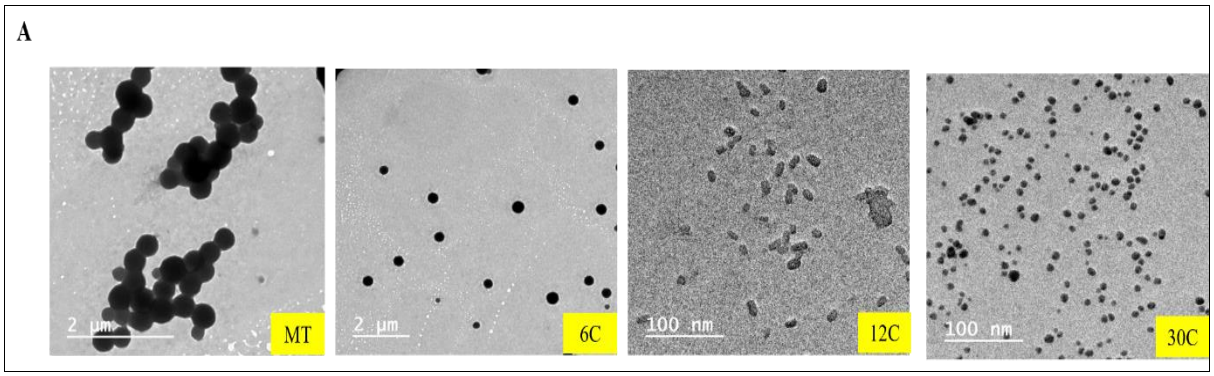

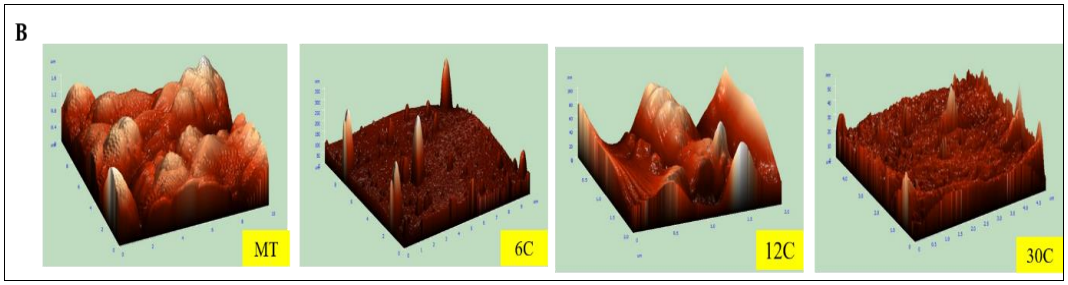

Fig 7: Physico-chemical characterization of MT and various dilutions of homeopathic formulation of CM. (A) TEM and (B) SPM images of the MT, 6C, 12C, and 30C dilutions of CM.

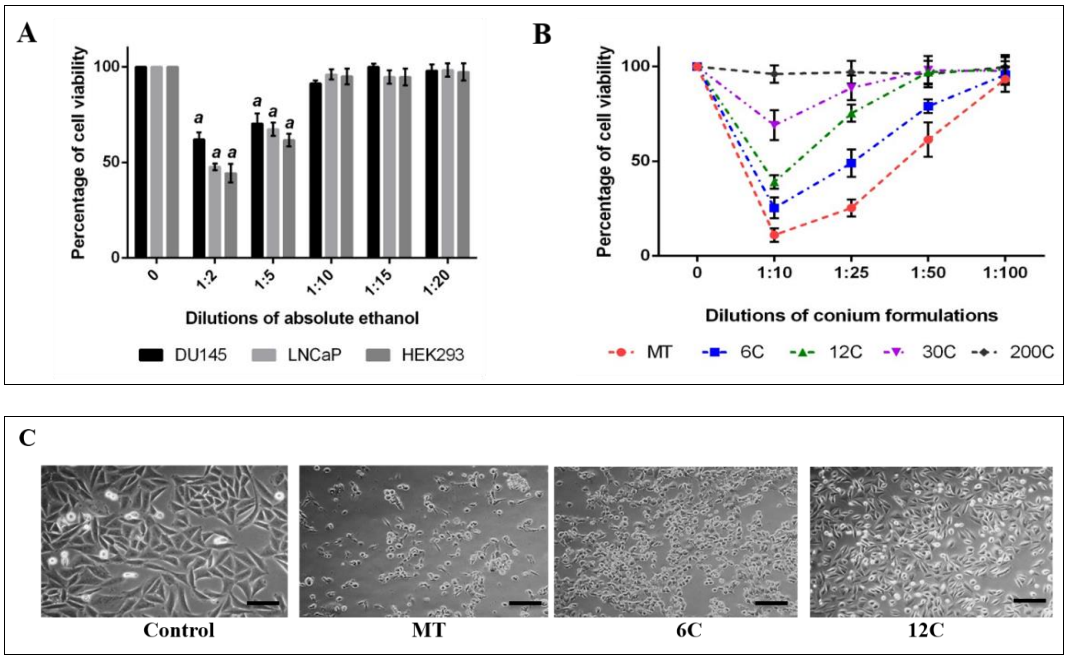

Fig 8: Anti-proliferative effect of various formulations of CM. Cytotoxicity assessment of different dilutions of (A) absolute ethanol and (B) various dilutions of CM by MTT assay. (C) Representative morphological images of the cells as observed through 10X objective. Results are mean ± SEM of three independent experiments. "a", indicates statistically significant at $p<0.05$ with respect to respective cell's control groups (0 dilution). Images are under 10X magnification. Scale bar 200 µm.

Table 1: MD simulated interaction energies (kJ/mol) between different protein molecules in both systems calculated at 298.15 K and 1 atm Pressure

Protein pair	Electrostatic Interactions (E_{elec})		VdW Interactions (E_{vdW})		Total Non-Bonded Interactions (E_{total})	
	S1	S2	S1	S2	S1	S2
COC-COH	-2.060	-2.671	-18.673	-19.724	-20.733	-22.395
COC-COI	-1.013	-1.078	-23.184	-23.956	-24.197	-25.034
COC-NME	-1.929	-1.582	-15.443	-14.994	-17.371	-16.577
COC-PSE	-1.535	-2.146	-15.087	-18.818	-16.622	-20.964
COH-COI	-5.520	-4.918	-20.571	-20.201	-26.091	-25.119
COH-NME	-5.705	-4.927	-18.197	-16.282	-23.902	-21.209
COH-PSE	-21.815	-27.924	-26.853	-29.423	-48.667	-57.348
COI-NME	-2.907	-2.366	-16.964	-15.585	-19.871	-17.952
COI-PSE	-4.979	-2.929	-18.013	-16.986	-22.992	-19.915
PSE-NME	-8.133	-9.018	-19.760	-22.019	-27.894	-31.037

Table 2: Total energy of both systems

System	KE (kJ/mol)	PE (kJ/mol)	Total Energy (kJ/mol)
S1 (initial)	8442.887	-12075.596	-3632.709
S1 (final)	8575.022	-14229.616	-5654.594
S2 (initial)	871.303	-1141.683	-270.380
S2 (final)	857.413	-1408.621	-551.208

Table 3: Self-diffusivity of different molecular protein species

Molecules species	Diffusion coefficient (D) × 10^{-9} m^2 s^{-1}					
	System S1			System S2		
	0−10 ns	40−50 ns	90−100 ns	0−10 ns	40−50 ns	90−100 ns
Conhydrine (COH)	0.1995	0.2177	0.1971	0.1232	0.1254	0.1220
Conicene (COC)	0.2257	0.2574	0.3210	0.1621	0.1557	0.1468
Coniine (COI)	0.2377	0.2177	0.2875	0.1411	0.1495	0.1523
Psedoconhydrine (PSE)	0.2247	0.2127	0.1774	0.1264	0.1152	0.1112
N-methylconniine(NME)	0.2511	0.2576	0.2775	0.1488	0.1440	0.1537

Table 4: IC_{50} estimation of different dilutions of CM in DU145 cells.

Dilutions	IC_{50}
MT	1:42 ± 0.022
6C	1:32 ± 0.024
12C	1:23 ± 0.030
30C	-
200C	-

5. Conclusions

This study introduces a novel method for examining the energy dynamics of homeopathic formulations, providing a partial elucidation of their mechanism of action, which has long been a subject of debate. The identified nanoparticulate nature of *Conium maculatum* (CM) formulations highlights a possible pathway for their therapeutic effects, especially in the context of prostate cancer treatment. Our findings demonstrate significant anti-proliferative effects against prostate cancer cells, supporting the potential of CM in clinical applications. However, these results are preliminary, and extensive further research is necessary to fully understand the mechanisms and validate the clinical efficacy of homeopathic remedies. This research paves the way for integrating such alternative treatments into mainstream medical practice, emphasizing the need for a rigorous scientific approach to explore the potential of homeopathy further.

Declarations

Funding: This work is supported by the research grant to PR from Ministry of AYUSH, Government of India [File no. Z.28015/04/2018-HPC (EMR)-AYUSH-D dated August 28, 2018]. ND was supported by DST-INSPIRE, Government of India, research fellowship (JRF/SRF) and contingency that assisted him in pursuing doctoral research.

Conflicts of interest: The authors declare that they have no conflicts of interest.

Acknowledgements: The authors would like to acknowledge the common instrument facility in the Department of Biotechnology, Indian Institute of Technology, Roorkee, Uttarakhand, India – 247667, for providing their FACS facility. The authors also acknowledge support from IIT Guwahati for the computational time in the PARAM ISHAN supercomputer for providing and executing necessary computational time for MD simulations through Dr. P.K. Naik and Dr. T. Banerjee.

References

1. Ferlay J, Soerjomataram I, Dikshit R, Eser S, Mathers C, Rebelo M, *et al*. Cancer incidence and mortality worldwide: Sources, methods and major patterns in GLOBOCAN 2012. International Journal of Cancer. 2015 Mar 1;136(5).
2. Schmidt JM. History and relevance of the 6th edition of the Organon of Medicine (1842). British Homeopathic Journal. 1994 Jan;83(01):42-8.
3. Tournier AL, Roberts ER, Viksveen P, Steinsbekk A. Prevalence of homeopathy use by the general population worldwide: a systematic review. Homeopathy. 2020 Aug;109(3):131-8.
4. Bell IR, Lewis DA 2nd, Brooks AJ, Schwartz GE, Lewis SE, Walsh BT, *et al*. Improved clinical status in fibromyalgia patients treated with individualized homeopathic remedies versus placebo. Rheumatology (Oxford). 2004 May;43(5):577-82.
5. Lenger K. Homeopathic potencies identified by a new magnetic resonance method: Homeopathy - an energetic medicine. Subtle Energies and Energy Medicine Journal Archives. 2006;15(3).
6. Shahabi S, Borneman JP. The electrostatic model of homeopathy: the mechanism of physicochemical activities of homeopathic medicines. Homeopathy. 2022;111(03):210-6.
7. Das N, Samantaray S, Ghosh C, Kushwaha K, Sircar D, Roy P. Chimaphila umbellata extract exerts anti-proliferative effect on human breast cancer cells via RIP1K/RIP3K-mediated necroptosis. Phytomedicine Plus. 2022 Feb 1;2(1):100159.
8. Frisch MJ, Trucks GW, Schlegel HB, *et al*. Gaussian 09, Revision E.01. Wallingford CT: Gaussian, Inc.; 2009.
9. Kohn W, Becke AD, Parr RG. Density functional theory of electronic structure. Journal of Physical Chemistry. 1996;100(31):12974-80.
10. Bayly CI, Cieplak P, Cornell W, Kollman PA. A well-behaved electrostatic potential based method using charge restraints for deriving atomic charges: the RESP model. Journal of Physical Chemistry. 1993;97(40):10269-80.
11. Case DA, *et al*. AMBER 14. San Francisco: University of California; c2014.
12. Wang J, Wolf RM, Caldwell JW, Kollman PA, Case DA. Development and testing of a general amber force field. Journal of Computational Chemistry. 2004;25(9):1157-74.
13. Wang J, Wolf RM, Caldwell JW, Kollman PA, Case DA. Development and testing of a general amber force field. Journal of Computational Chemistry. 2004;25(9):1157-74.
14. Paul N, Naik PK, Ribeiro BD, Gooh Pattader PS, Marrucho IM, Banerjee T. Molecular dynamics insights and water stability of hydrophobic deep eutectic solvents aided extraction of nitenpyram from an aqueous environment. Journal of Physical Chemistry B. 2020 Jul 24;124(34):7405-20.

15. Naik PK, Paul S, Banerjee T. Physiochemical properties and molecular dynamics simulations of phosphonium and ammonium based deep eutectic solvents. Journal of Solution Chemistry. 2019 Jul 31;48:1046-65.
16. Kumar N, Naik PK, Banerjee T. Molecular modeling insights in the extraction of benzene from hydrocarbon stream using deep eutectic solvent. Journal of Molecular Liquids. 2020 Nov 1;317:113909.
17. Naik PK, Mohan M, Banerjee T, Paul S, Goud VV. Molecular dynamic simulations for the extraction of quinoline from heptane in the presence of a low-cost phosphonium-based deep eutectic solvent. Journal of Physical Chemistry B. 2018 Mar 15;122(14):4006-15.
18. Tournier AL, Roberts ER, Viksveen P, Steinsbekk A. The role of homeopathy in modern health care. Homeopathy. 2021;110(2):123-130.
19. Boericke W. Homeopathic Materia Medica. Philadelphia: Boericke & Tafel; 2004.
20. Bellavite P, Chirumbolo S, Santonastaso C, Biasi D, Lussignoli S, Andrioli G. Complexity in the science of homeopathy. Homeopathy. 2014 Jul;103(3):123-129.
21. Preparata G, Vitiello G. Quantum coherence in water and its role in homeopathy. Homeopathy. 1988 Jul;77(3):182-195.
22. Wani A, Das S, Mukherjee SP, Iqbal M, Vishwakarma R, Vijayakumar R. Nanoparticle characterization of traditional homeopathically prepared Terminalia chebula. Homeopathy. 2016;105(1):54-58.
23. Klein SD, Wolf U. Nanoparticles in homeopathic preparations. Homeopathy. 2013 Apr;102(2):112-117.
24. Baumgartner S, Heusser P, Thurneysen A. Nanoparticulate nature of homeopathic remedies. Langmuir. 2009;25(19):11624-11629.
25. Upadhyay RP, Nayak C. Homeopathy: Treatment of cancer with highly diluted preparations. Journal of Alternative and Complementary Medicine. 2011 Oct;17(10):891-899.
26. Castells E, Berdonces JL, Borràs JM, Brotons M, Cardús J, Casafont M. Analysis of active components in CM extracts. Homeopathy. 2005 Jan;94(1):10-16.
27. Radulović NS, Đorđević MS. Analytical studies on active compounds in CM. Analytical and Bioanalytical Chemistry. 2011 Oct;400(9):2813-2828.
28. Mondal J, Samadder A, Banerjee R, Mondal J, Das S, Khuda-Bukhsh AR, *et al*. Anticancer properties of CM extracts. Homeopathy. 2014 Apr;103(2):97-102.
29. Bishayee A, Sethi G, Kundu A, Thoppil RJ, Darvesh AS, Sikdar S, *et al*. Therapeutic effectiveness of CM in cancer treatment. International Journal of Oncology. 2014 Mar;44(3):897-904.

How to Cite This Article
Das N, Naik PK, Ghosh C, Raj A, Sircar D, Banerjee T, Roy P. Physico-chemical characterization, energy dynamics and anti-cancer efficacy of *Conium maculatum* homeopathic formulations against prostate cancer cell lines. International Journal of Homoeopathic Sciences. 2024; 8(2): 485-497.

Supplementary Method1: Methodology for molecular simulation:

Classical molecular dynamics simulations were conducted for two systems, S1 and S2. S1 contained 100 molecules of each protein species without external force, while S2 contained 10 molecules of each species with a randomly applied external force (Supplementary Table 1). S1's simulation box was set up at high density, whereas S2's was at low density with molecules arranged using PACKMOL [1]. Both systems underwent molecular dynamics (MD) simulations at 289.15 K using the NAnoscale Molecular Dynamics (NAMD) 2.9 package [2]. Temperature and pressure were regulated using Langevin thermostat [3] and Nose-Hoover Langevin barostat [4].

Initially, both systems underwent a minimization step for 6 nanoseconds using the conjugate gradient method (NVT ensembles), followed by heating to 298.15 K within 0.2 ns. They were then equilibrated for 6 ns in NPT ensemble at 298.15 K and atmospheric pressure, maintaining static temperature using Langevin dynamics with a collision frequency of 1 ps−1 [5]. The pressure was managed using Nose-Hoover Langevin piston with a 100 fs oscillation period and a 50 fs damping factor [6]. The production run lasted 100 ns for both systems using NVT ensemble, with time integration of 1 fs. The SHAKE algorithm was employed to enforce bond length constraints involving all hydrogen atoms [7], and periodic boundary conditions were applied to minimize edge effects [8]. The Particle mesh Ewald (PME) method [9] was used for long-range electrostatic interactions, with a 12 Å cutoff for short-range interactions.

Simulation data were saved every 5 ps for analysis using the Visual Molecular Dynamics (VMD) 1.9.3 package [10]. The TRAVIS package [11] was utilized to generate spatial distribution function (SDF) visuals with proper isovalue. Self-diffusivity values were determined from the mean square displacement (MSD) curve, following Einstein's equation via the VMD console.

Supplementary Table 1. System compositions for MD Simulations for different systems

System	S1	S2
Conhydrin (COH)	100	10
Coniceine (COC)	100	10
Coniine (COI)	100	10
Pseudoconhydrine (PSE)	100	10
N-methylconniine (NME)	100	10
Total numbers	500	50
Random Force	No	Yes
Initial box dimension	(50Åx50Åx50Å)	(25Åx25Åx25Å)

Final equilibrated box dimension	(48.75Åx48.75Åx48.75Å)	(22.67Åx22.67Åx22.67Å)
System density (g/cm^3)	0.8582	0.6865